

You Do Not Need Additional Priors in Camouflage Object Detection

Yuchen Dong
dongyc91@outlook.com
Academy of Military Sciences
Beijing, China

Heng Zhou
School of Electronic Engineering,
Xidian University
Xi'an, China
hengzhou@stu.xidian.edu.cn

Chengyang Li
School of Computer Science, Peking
University
Beijing, China
chengyang_li@stu.pku.edu.cn

Junjie Xie
Academy of Military Sciences
Beijing, China
xiejunjie06@gmail.com

Yongqiang Xie
Academy of Military Sciences
Beijing, China
yqxie.ams@gmail.com

Zhongbo Li
Academy of Military Sciences
Beijing, China
zbli83@foxmail.com

ABSTRACT

Camouflage object detection (COD) poses a significant challenge due to the high resemblance between camouflaged objects and their surroundings. Although current deep learning methods have made significant progress in detecting camouflaged objects, many of them heavily rely on additional prior information. However, acquiring such additional prior information is both expensive and impractical in real-world scenarios. Therefore, there is a need to develop a network for camouflage object detection that does not depend on additional priors. In this paper, we propose a novel adaptive feature aggregation method that effectively combines multi-layer feature information to generate guidance information. In contrast to previous approaches that rely on edge or ranking priors, our method directly leverages information extracted from image features to guide model training. Through extensive experimental results, we demonstrate that our proposed method achieves comparable or superior performance when compared to state-of-the-art approaches.

CCS CONCEPTS

• Computing methodologies → Interest point and salient region detections; Computer vision tasks.

KEYWORDS

Camouflage object detection, Without additional priors, Adaptive feature aggregation.

1 INTRODUCTION

Camouflaged object detection is a research field that focuses on the identification of camouflaged objects within images [1, 2]. Specifically, camouflaged objects can be categorized into natural camouflage and artificial camouflage [3]. Natural camouflage refers to how organisms utilize properties such as brightness, color, and body shape to conceal themselves in their environment [4]. Many species employ this strategy as a means of survival, either to avoid predators or to capture prey [5, 6]. On the other hand, artificial camouflage involves the use of techniques such as paint, clothing, and accessories to create visual deception and conceal the object. This form of camouflage is commonly employed in military applications [7, 8], art [9], and other domains [10, 11]. The primary

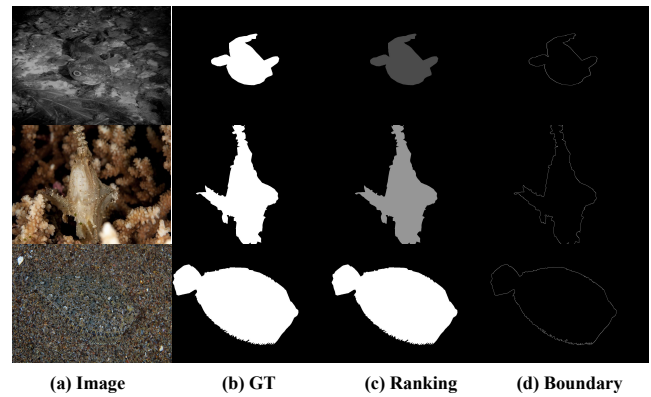


Figure 1: We introduce two common types of additional prior information: boundary priors and ranking priors. Specifically, the boundary prior refers to boundary information about the concealed object, while the ranking prior includes information predefined based on the overall difficulty of human observation of the concealed object.

objective of camouflaged object detection is to generate a binary detection map for the camouflaged objects present in the image [3]. However, detecting camouflage presents a challenge due to the visual similarity between the foreground and background [12–14].

Some recent studies [15, 16] have tackled the challenge of detecting camouflaged objects by incorporating additional priors. These researchers argue that relying solely on image features for training is insufficient to accurately identify boundary information and comprehend camouflaged objects [15]. Fig. 1 illustrates common additional priors, including boundary and rank information. Specifically, [16] utilized boundary information to enhance the model’s ability to detect object edges, while [15] employed rank information to assist the model in understanding the evolution of camouflaged objects and animals. However, it is crucial to note that manual annotation is required for these additional priors, which increases the implementation cost of utilizing such models.

To tackle this challenge, we introduce a novel adaptive feature fusion module (AFFM) that generates guidance information. Our

objective is to utilize the guidance information derived from image features to guide the model’s learning process, eliminating the need for additional priors. The AFFM is designed to effectively combine and integrate features from different network layers, enabling the model to exploit the inherent relationships among these features. Additionally, we propose a **Progressive Feature Refinement Network (PFRNet)** that utilizes the guidance information to direct the model in the progressive refinement of image features. Through extensive experiments, we provide compelling evidence of the effectiveness and robustness of our proposed approach.

Overall, our work makes the following main contributions:

- Firstly, we introduce an adaptive feature fusion module that extracts guidance information directly from image features, eliminating the need for additional priors.
- Secondly, we propose a novel PFRNet that enhances the performance of camouflaged object detection by leveraging guidance information to refine the image features.
- Thirdly, we introduce two modules: the Feature Refinement Module (FRM) and the Context-Aware Feature Decoding Module (CFDM). These modules utilize the guidance information to refine features, guide model training, and efficiently integrate the refined features using a cross-channel approach, resulting in precise predictions.

2 RELATED WORK

Camouflage Object Detection. In recent years, COD methods can be categorized into two groups: those utilizing prior information and those not relying on prior information.

With addition prior. *Lv et al.* [15] introduced a joint framework for locating, segmenting, and ranking camouflaged objects. They incorporated additional ranking information during training, which improved the understanding of camouflage. *Zhai et al.* [17] proposed mutual graph learning, which effectively separates images into task-specific feature maps for precise localization and boundary refinement. *Sun et al.* [18] explored the use of object-related edge semantics as an additional guide for model learning, encouraging the generation of features that emphasize the object’s edges. *He et al.* [19] suggested using edge likelihood maps for guiding the fusion of camouflaged object features, aiming to enhance detection performance by improving boundary details. *Kajiura et al.* [16] employed a pseudo-edge generator to predict edge labels, contributing to accurate edge predictions. *Zhu et al.* [20] proposed the utilization of Canny edge [21] and ConEdge techniques to assist in model training. *Li et al.* [22] proposed co-training camouflage and saliency objects [23, 24] to enhance model detection. *Yang et al.* [1] integrated the advantages of Bayesian learning and transformer-based [25, 26] inference. They introduced Uncertainty-Guided Random Masking as prior knowledge to facilitate model training. However, prior information is often expensive and impractical.

Without additional prior. *Mei et al.* [27] proposed a localization module, a focus module, and a novel distraction mining strategy to enhance model performance. *Fan et al.* [3, 28] introduced a search and recognition network inspired by the predatory behavior of hunters in nature, which implements object localization and recognition steps. *Sun et al.* [29] proposed an attention-inducing fusion module that integrates multi-level features and incorporates

contextual information for more effective prediction. *Zhang et al.* [6] proposed a model that incorporates two processes of predation, specifically sensory and cognitive mechanisms. To achieve this, specialized modules were designed to selectively and attentively aggregate initial features using an attention-based approach. *Jia et al.* [30] proposed a method where the model attends to fixation and edge regions and utilizes an attention-based sampler to progressively zoom in on the object region instead of increasing the image size. This approach allows for the iterative refinement of features. In practice, algorithms that do not depend on prior information typically utilize various techniques to aggregate features with different receptive field sizes to obtain better detection results. While these algorithms are cost-effective, they often face limitations in efficiently mining image information. In contrast, our proposed PFRNet generates guidance information by extracting valuable features from the image itself without relying on prior information, thereby effectively guiding the model training process.

3 PROPOSED METHOD

3.1 Overall Architecture

The architecture of PFRNet is illustrated in Fig. 2, which consists of three modules: adaptive feature fusion module (AFFM), feature refinement module (FRM), and context-aware feature decoding module (CFDM), as described in Sec. 3.2, Sec. 3.3 and Sec. 3.4 respectively. For extracting multi-scale features, the Res2Net-50 [31] architecture is utilized as the backbone. In this paper, the multi-scale features are obtained from the last four layers of the feature hierarchy. The layer closest to the input is excluded as it contains excessive noise and has a small receptive field. Please note that the layer closest to the input is not depicted in Fig. 2.

3.2 Adaptive Feature Fusion Module

The boundary prior is used to aid the object detection model in localizing and segmenting objects [32]. However, the necessary information for localization and segmentation is already present in the image features. Additional prior information is utilized because the image features often contain significant noise, which makes it challenging for previous models to extract reliable feature information. In our proposed module, we employ an adaptive feature fusion approach that learns the relationships between different feature layers. This enables the effective fusion of features by considering the importance of each layer. As a result, we prioritize the most discriminative and complementary information from each layer while suppressing noisy and irrelevant features. Specifically, AFFM combines high-level features $\{f_i\}_{i=2}^4$ and low-level features f_1 to generate effective global guidance information. This global guidance information assists the features at each layer in complementing missing information.

In Fig. 2, the AFFM is depicted, which consists of two branches. Firstly, applying a convolution operation to all input features. Subsequently, the higher-level features are upsampled to achieve a uniform size $\{x_i\}_{i=1}^3 \in \mathbb{R}^{\frac{H}{8} \times \frac{W}{8} \times 256}$. The feature maps of the same size undergo the deep layer attention (DLA) [33] operation, which explores the interrelationships between different layers. The resulting features are aggregated to produce $x_h \in \mathbb{R}^{\frac{H}{8} \times \frac{W}{8} \times 768}$. The

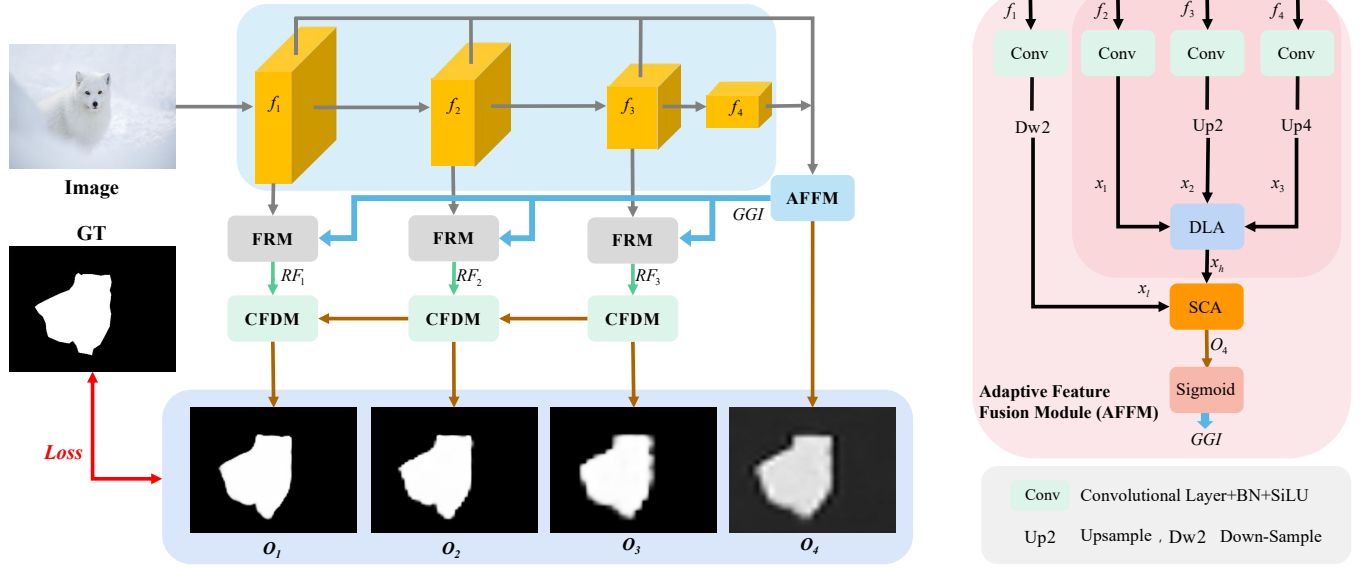


Figure 2: Overview of our framework. The proposed PFRNet framework comprises three novel components: the adaptive feature fusion module (AFFM), the feature refinement module (FRM), and the context-aware feature decoding module (CFDM). The AFFM is responsible for learning the correlations between multi-layer features and adaptively fusing them to generate reliable guidance information. This guidance information is robust enough to replace the need for additional prior information during model training. The FRM utilizes the guidance information to refine image features, while the CFDM considers the relationships between different branches of the same feature and decodes features top-down, incorporating contextual semantics across channels.

computation process of DLA is represented by Eq. 1.

$$\begin{aligned}
 w_{i,j} &= \text{Softmax}(\phi(x)_i \cdot (\phi(x))_j^T), i, j \in \{1, 2, 3\} \\
 x_j &= \beta \sum_{i=1}^3 w_{i,j} x_i + x_j, x_i/x_j \in \{x_1, x_2, x_3\} \\
 x_h &= [x_1; x_2; x_3]
 \end{aligned} \quad (1)$$

where $w_{i,j}$ represents the correlation weight between layer i and layer j , $\phi(\cdot)$ denotes the reshape operations, and β is initially set to 0 and then automatically assigned by the network.

To derive feature $x_l \in \mathbb{R}^{\frac{H}{8} \times \frac{W}{8} \times 128}$ from the low-level feature f_1 , we use operations involving 1×1 convolution and downsampling. Subsequently, a spatial channel attention (SCA) operation is performed on features x_l and x_h , resulting in the feature $O_4 \in \mathbb{R}^{\frac{H}{8} \times \frac{W}{8} \times 1}$. This O_4 feature is one of the output features generated by the model. The above process can be described as follows:

$$\begin{aligned}
 x_l &= \text{Conv}_{1 \times 1}(f_1) \\
 O_4 &= \text{SCA}(x_l, x_h) \\
 \text{SCA} &\Leftarrow \text{Conv}_{1 \times 1}(\text{Conv}_{3 \times 3}(\text{CBAM}(\text{Conv}_{1 \times 1}(\cdot))))
 \end{aligned} \quad (2)$$

Where $\text{Conv}_{i \times i}$ represents a set of convolution operations with a convolution kernel size of $i \times i$, a BN (Batch Normalization) layer, and a SiLU activation function. We apply CBAM [34] to extract features from both the spatial and channel dimensions. Finally, a sigmoid calculation is performed on the resulting feature O_4 to obtain the global guide information (GGI).

The integration of high and low-level features in the AFFM module enables a more comprehensive understanding of the image. By combining features from different layers, the model can leverage the unique strengths of each layer. This adaptive fusion process ensures that the generated guidance information provides valuable guidance during the model's training process, utilizing discriminative and complementary information from the various feature layers. The fusion of features enhances the model's capacity to capture relevant information, thereby improving its performance in camouflaged object detection tasks.

3.3 Feature Refinement Module

As mentioned, the AFFM module extracts relevant object details from image features to achieve a comprehensive understanding of the entire image, generating global guidance information (GGI). In the feature refinement module (FRM), we incorporate the generated GGI into the model to guide the training of the detection model. Specifically, we utilize GGI to refine the image features at each layer, complementing the missing information in each layer of features. Fig. 3 provides an overview of the overall structure of the FRM.

In FRM, the image features $\{f_i\}_{i=1}^3$ undergo channel attention (CA) [35] to learn cross-channel correlations, enhancing the expressiveness of the features. Subsequently, a convolution operation is applied to reduce the number of feature channels, resulting in coarse feature $g_{coarse} \in \mathbb{R}^{\frac{H}{2^{i+1}} \times \frac{W}{2^{i+1}} \times 256}$. Simultaneously, feature GGI performs (up/down) sampling operations to obtain feature

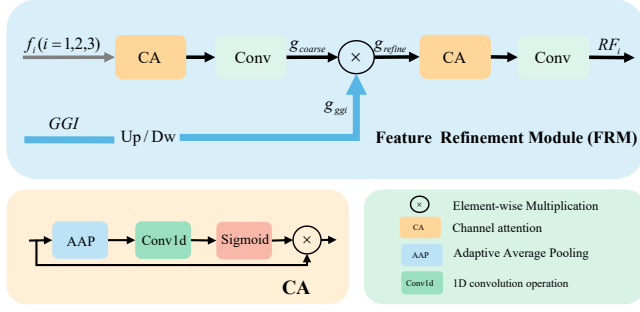


Figure 3: Illustrate of FRM. FRM uses *GGI* to refine the image features and complement the missing information in each layer of features. The guidance provided by *GGI* assists the entire network in conducting a more comprehensive image content analysis.

$g_{ggi} \in \mathbb{R}^{\frac{H}{2^{i+1}} \times \frac{W}{2^{i+1}} \times 1}$. The refinement features g_{refine} is obtained by element-wise multiplying g_{coarse} and g_{ggi} . Finally, features $\{RF_i\}_{i=1}^3$ are calculated by applying CA and convolution operations to g_{refine} . The calculation process is depicted in Eq. 3.

$$\begin{aligned} g_{coarse} &= Conv_{3 \times 3}(CA(f_i)), i \in \{1, 2, 3\} \\ g_{refine} &= g_{coarse} \otimes Up2/Dw2(g_{ggi}) \\ RF_i &= Conv_{1 \times 1}(CA(g_{refine})), i \in \{1, 2, 3\} \end{aligned} \quad (3)$$

where f_i represents the image features output by the backbone. RF_i is the refined feature.

3.4 Context-aware Feature Decoding Module

To integrate the contextual features and generate informative predictive binary maps, we introduce the context-aware feature decoding module (CFDM). In contrast to the Texture Enhanced Module (TEM) [3], our approach considers the semantic correlation between different branches within the same layer of features. As shown in Fig. 4, we obtain features $\{y_i\}_{i=1}^3 \in \mathbb{R}^{\frac{H}{2^{i+1}} \times \frac{W}{2^{i+1}} \times 256}$ by aggregating the fine features $\{RF_i\}_{i=1}^3$ and the high-level output features $\{O_i\}_{i=2}^3$ through preprocessing operation (PPO). The feature $\{y_i\}_{i=1}^3$ comprises top-down semantic information and is subsequently divided equally into four parts $[y_i^1; y_i^2; y_i^3; y_i^4]$ in the channel dimension. The generation process of $\{y_i\}_{i=1}^3$ is illustrated in Eq. 4.

$$\begin{aligned} y_i &= PPO(RF_i, O_{i+1}), i \in \{1, 2\} \\ y_3 &= RF_3 \end{aligned} \quad (4)$$

After obtaining the feature y_i^j , we add the features of a branch to the features of its neighboring branches. This process can be formulated as follows:

$$\begin{aligned} z_i^1 &= CB_1(y_i^1 + y_i^2), i \in \{1, 2, 3\} \\ z_i^j &= CB_j(z_i^{j-1} + y_i^j + y_i^{j+1}), i \in \{1, 2, 3\}, j \in \{2, 3\} \\ z_i^4 &= CB_4(z_i^3 + y_i^4), i \in \{1, 2, 3\} \end{aligned} \quad (5)$$

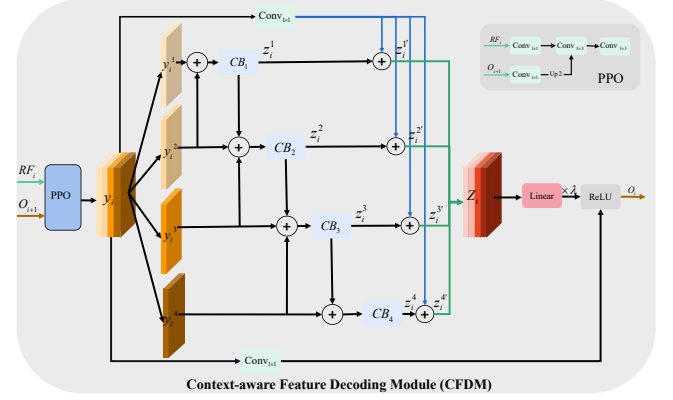


Figure 4: Illustration of CFDM. CFDM obtains multi-scale contextual features between adjacent features through cross-channel interaction learning, enhancing the feature representation.

where $\{CB_j\}_{j=1}^4$ indicates a series of convolution operations and the specific composition of $\{CB_j\}_{j=1}^4$ is shown in Eq. 6.

$$\begin{aligned} CB_1 &\Leftarrow DConv_{3 \times 3}^1(Conv_{1 \times 1}(\cdot)) \\ CB_2 &\Leftarrow DConv_{3 \times 3}^3(Conv_{3 \times 1}(Conv_{1 \times 1}(\cdot))) \\ CB_3 &\Leftarrow DConv_{3 \times 3}^3(Conv_{1 \times 3}(Conv_{1 \times 1}(\cdot))) \\ CB_4 &\Leftarrow DConv_{3 \times 3}^5(Conv_{1 \times 3}(Conv_{3 \times 1}(Conv_{1 \times 1}(\cdot)))) \end{aligned} \quad (6)$$

where $DConv_{i \times i}^j$ represents a atrous convolution [36] with a convolution kernel size of $i \times i$ and a dilation rate of j .

Subsequently, we apply residual connections on each branch to obtain the feature $z_i^j \in \mathbb{R}^{\frac{H}{2^{i+1}} \times \frac{W}{2^{i+1}} \times 256}$. Then, we merge all z_i^j to generate the feature $\{Z_i\}_{i=1}^3 \in \mathbb{R}^{\frac{H}{2^{i+1}} \times \frac{W}{2^{i+1}} \times 256}$. Finally, we use a linear function, ReLU function, and a residual connection to obtain output feature $\{O_i\}_{i=1}^3 \in \mathbb{R}^{\frac{H}{2^{i+1}} \times \frac{W}{2^{i+1}} \times 1}$. The scaling factor $\lambda = 0.5$ is employed in this process.

3.5 Loss Function

PFRNet incorporates two types of loss functions: dice loss (L_{dice}) [10] and structural loss (L_{struct}) [38]. For O_4 , we utilize L_{dice} to balance scenarios where positive and negative samples are unbalanced. For $\{O_i\}_{i=1}^3$, we apply L_{struct} to promote structural consistency and accuracy.

$$L_{struct} = L_{BCE}^w + L_{IoU}^w \quad (7)$$

Therefore, the total loss is defined as in Eq. 8.

$$L_{total} = \sum_{i=1}^3 L_{struct}(O_i, GT) + L_{dice}(O_4, GT) \quad (8)$$

where $\{O_i\}_{i=1}^4$ represents the feature map generated by PFRNet, and GT refers to the ground truth. During the testing process, O_1 is used as the prediction result of the model.

Table 1: Quantitative comparison with state-of-the-art methods for COD on three benchmarks using four widely used evaluation metrics (i.e., S_α , E_ϕ , F_β^w , and \mathcal{M}). The best scores are highlighted in Bold, and the symbol \uparrow indicates that a higher score is better.

Method	CAMO-Test				COD10K-Test				NC4K			
	$S_\alpha \uparrow$	$E_\phi \uparrow$	$F_\beta^w \uparrow$	$\mathcal{M} \downarrow$	$S_\alpha \uparrow$	$E_\phi \uparrow$	$F_\beta^w \uparrow$	$\mathcal{M} \downarrow$	$S_\alpha \uparrow$	$E_\phi \uparrow$	$F_\beta^w \uparrow$	$\mathcal{M} \downarrow$
2019 EGNNet [32]	0.732	0.800	0.604	0.109	0.736	0.810	0.517	0.061	0.777	0.841	0.639	0.075
2019 SCRNet [37]	0.779	0.797	0.643	0.090	0.789	0.817	0.575	0.047	0.830	0.854	0.698	0.059
2020 F ³ NET [38]	0.711	0.741	0.564	0.109	0.739	0.795	0.544	0.051	0.780	0.824	0.656	0.070
2020 CSNET [39]	0.771	0.795	0.642	0.092	0.778	0.809	0.569	0.047	0.750	0.773	0.603	0.088
2020 BASNET [40]	0.749	0.796	0.646	0.096	0.802	0.855	0.677	0.038	0.817	0.859	0.732	0.058
2020 SINet [28]	0.745	0.804	0.644	0.092	0.776	0.864	0.631	0.043	0.808	0.871	0.723	0.058
2021 PFNet [27]	0.782	0.841	0.695	0.085	0.800	0.877	0.660	0.040	0.829	0.887	0.745	0.053
2021 S-MGL [17]	0.772	0.806	0.664	0.089	0.811	0.844	0.654	0.037	0.829	0.862	0.731	0.055
2021 C ² FNet [29]	0.799	0.851	0.710	0.078	0.811	0.886	0.669	0.038	0.843	0.899	0.757	0.050
2022 BGNNet [18]	0.807	0.861	0.742	0.072	0.829	0.898	0.719	0.033	0.849	0.903	0.785	0.045
PFRNet (Ours)	0.827	0.877	0.754	0.069	0.833	0.888	0.710	0.033	0.859	0.902	0.785	0.045

4 EXPERIMENTS AND ANALYSIS

4.1 Experiment Setup

We implement our model using PyTorch and utilize the Adam optimization algorithm [41] to optimize the overall parameters. The learning rate starts at $1e^{-4}$, dividing by 10 every 50 epochs. The model is accelerated using an NVIDIA 3090Ti GPU. During the training stage, the batch size is set to 36, and the whole training takes approximately 100 epochs.

4.2 Comparison with State-of-the-arts

We evaluate our method on three benchmark datasets: CAMO [42], COD10K [28], and NC4K [15]. And we use four widely used and standard metrics to evaluate our method: MAE (\mathcal{M}) [24], weighted F-measure (F_β^w) [43], average E-measure (E_ϕ) [44] and S-measure (S_α) [45].

To demonstrate the effectiveness of our proposed PFRNet, we conducted a comparative analysis by comparing its prediction results with those of ten state-of-the-art methods. The selected methods for comparison are EGNNet[32], SCRNet [37], F³Net [38], CSNet [39], BASNet [40], SINet [28], PFNet [27], S-MGL [17], BGNNet [18] and C²FNet [29]. For a fair comparison, the prediction results of these methods were provided by the original authors or generated using models trained with open-source code.

Quantitative Evaluation Table 1 summarizes the quantitative results of different COD methods on the three benchmark datasets. Our method outperforms previous methods in all four evaluation indicators on the three datasets. In particular, compared with the BGNNet [18], our method shows an average increase of 1.13% in S_α , 0.16% in E_ϕ , and 0.1% in F_β^w .

Regarding the slightly lower training results compared to BGNNet for some datasets, we have analyzed the reasons behind these differences. We attribute them to two main factors. Firstly, during supervised learning, we did not incorporate additional priors, which may have influenced the detection performance of our model. The absence of these additional priors might have affected the model’s

ability to capture certain intricate details and characteristics of the objects. Secondly, as illustrated in Fig. 5, when comparing the prediction results of PFRNet with those of other models, we observed that PFRNet effectively addressed the issue of uneven pixel distribution. However, this occasionally led to an expanded range of predicted objects, which might have impacted specific evaluation metrics. For instance, in the first row of Fig. 5, the leg of the animal and in the fifth row, the size of the people were slightly affected.

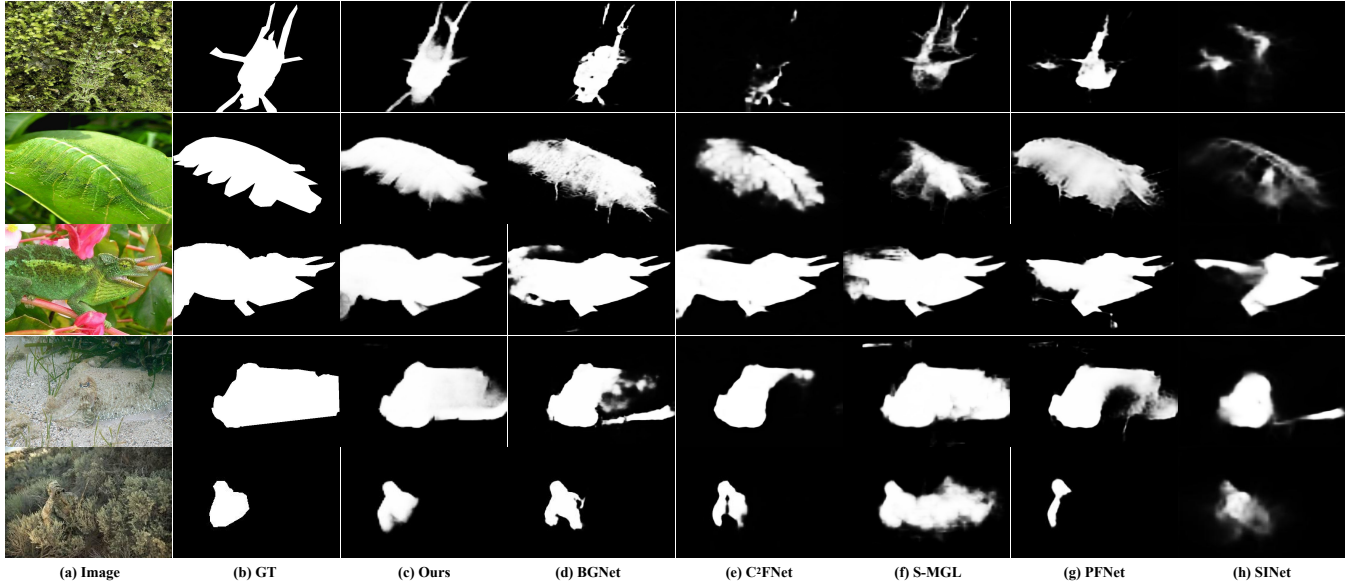
Qualitative Evaluation Fig. 5 shows a qualitative comparison of different COD methods on the CAMO dataset. Compared to several other state-of-the-art models, our proposed PFRNet effectively addresses the issue of uneven image distribution. This can be observed in the fourth and fifth rows of Fig. 5, where PFRNet’s predictions exhibit improved completeness and accuracy regarding boundary processing, leading to visually superior results. Furthermore, this comparison highlights the effectiveness of our adaptive feature fusion approach in extracting valuable edge information. Our model achieves superior edge detection performance without requiring additional edge prior guidance.

5 CONCLUSION

In this paper, we propose a novel network called PFRNet for camouflaged object detection, with the goal of reducing the reliance on additional priors. Our proposed method introduces an adaptive feature fusion module that generates guidance information, eliminating the need for additional priors to guide model training. Additionally, we introduce two modules, FRM and CFDM, which leverage guidance information to complement missing features in image representations and enhance feature representation by incorporating contextual information. Through extensive evaluations on three benchmark datasets, we demonstrate that our approach achieves state-of-the-art performance.

Table 2: Quantitative evaluation for ablation studies on three datasets. The best results are highlighted in Bold.

No.	Method	CAMO-Test				COD10K-Test				NC4K			
		$S_\alpha \uparrow$	$E_\phi \uparrow$	$F_\beta^w \uparrow$	$M \downarrow$	$S_\alpha \uparrow$	$E_\phi \uparrow$	$F_\beta^w \uparrow$	$M \downarrow$	$S_\alpha \uparrow$	$E_\phi \uparrow$	$F_\beta^w \uparrow$	$M \downarrow$
A	Base	0.799	0.860	0.717	0.078	0.801	0.867	0.655	0.038	0.834	0.887	0.745	0.050
B	Base+CFDM	0.814	0.852	0.727	0.078	0.827	0.875	0.690	0.034	0.854	0.892	0.771	0.046
C	Base+AFFM+FRM	0.818	0.870	0.746	0.072	0.832	0.885	0.710	0.032	0.852	0.903	0.782	0.045
D	Base+FRM+CFDM	0.822	0.864	0.745	0.074	0.827	0.871	0.694	0.035	0.855	0.892	0.773	0.047
E (ours)	Base+AFFM+FRM+CFDM	0.827	0.877	0.754	0.069	0.833	0.888	0.710	0.033	0.859	0.902	0.785	0.045

**Figure 5: Visual comparison of the proposed model with five state-of-the-art COD methods.****Table 3: Sensitivity analysis on λ . We compared the best scale factors using the four widely used indicators on three datasets. The best results are highlighted in Bold.**

No.	λ	CAMO-Test				COD10K-Test				NC4K			
		$S_\alpha \uparrow$	$E_\phi \uparrow$	$F_\beta^w \uparrow$	$M \downarrow$	$S_\alpha \uparrow$	$E_\phi \uparrow$	$F_\beta^w \uparrow$	$M \downarrow$	$S_\alpha \uparrow$	$E_\phi \uparrow$	$F_\beta^w \uparrow$	$M \downarrow$
I	0.2	0.817	0.863	0.740	0.075	0.830	0.877	0.705	0.033	0.855	0.898	0.781	0.045
II	0.3	0.826	0.875	0.753	0.070	0.832	0.884	0.703	0.032	0.857	0.899	0.785	0.044
III	0.4	0.825	0.869	0.750	0.070	0.832	0.885	0.708	0.032	0.855	0.897	0.782	0.045
IV	0.5	0.827	0.877	0.754	0.069	0.833	0.888	0.710	0.033	0.859	0.902	0.785	0.045
V	0.6	0.815	0.865	0.738	0.076	0.832	0.888	0.706	0.033	0.857	0.901	0.784	0.045

Table 4: Quantitative evaluation for ablation studies on three datasets. The best results are highlighted in Bold.

No.	Method	CAMO-Test				COD10K-Test				NC4K			
		$S_\alpha \uparrow$	$E_\phi \uparrow$	$F_\beta^w \uparrow$	$M \downarrow$	$S_\alpha \uparrow$	$E_\phi \uparrow$	$F_\beta^w \uparrow$	$M \downarrow$	$S_\alpha \uparrow$	$E_\phi \uparrow$	$F_\beta^w \uparrow$	$M \downarrow$
A	Base	0.799	0.860	0.717	0.078	0.801	0.867	0.655	0.038	0.834	0.887	0.745	0.050
B	Base+CFDM	0.814	0.852	0.727	0.078	0.827	0.875	0.690	0.034	0.854	0.892	0.771	0.046
C	Base+AFFM+FRM	0.818	0.870	0.746	0.072	0.832	0.885	0.710	0.032	0.852	0.903	0.782	0.045
D	Base+FRM+CFDM	0.822	0.864	0.745	0.074	0.827	0.871	0.694	0.035	0.855	0.892	0.773	0.047
E (ours)	Base+AFFM+FRM+CFDM	0.827	0.877	0.754	0.069	0.833	0.888	0.710	0.033	0.859	0.902	0.785	0.045

REFERENCES

- [1] Fan Yang, Qiang Zhai, Xin Li, Rui Huang, Ao Luo, Hong Cheng, and Deng-Ping Fan. Uncertainty-guided transformer reasoning for camouflaged object detection. In *Proceedings of the IEEE/CVF International Conference on Computer Vision*, pages 4146–4155, 2021.
- [2] Chunming He, Kai Li, Yachao Zhang, Longxiang Tang, Yulun Zhang, Zhenhua Guo, and Xiu Li. Camouflaged object detection with feature decomposition and edge reconstruction. In *Proceedings of the IEEE/CVF Conference on Computer Vision and Pattern Recognition*, pages 22046–22055, 2023.
- [3] Deng-Ping Fan, Ge-Peng Ji, Ming-Ming Cheng, and Ling Shao. Concealed object detection. *IEEE Transactions on Pattern Analysis and Machine Intelligence*, 44(10):6024–6042, 2021.
- [4] Tom Troscianko, Christopher P Benton, P George Lovell, David J Tolhurst, and Zygmont Pizlo. Camouflage and visual perception. *Philosophical Transactions of the Royal Society B: Biological Sciences*, 364(1516):449–461, 2009.
- [5] Innes C Cuthill, Martin Stevens, Jenna Sheppard, Tracey Maddocks, C Alejandro Párraga, and Tom S Troscianko. Disruptive coloration and background pattern matching. *Nature*, 434(7029):72–74, 2005.
- [6] Miao Zhang, Shuang Xu, Yongri Piao, Dongxiang Shi, Shusen Lin, and Huchuan Lu. Preynet: Preying on camouflaged objects. In *Proceedings of the 30th ACM International Conference on Multimedia*, pages 5323–5332, 2022.
- [7] Yunfei Zheng, Xiongwei Zhang, Feng Wang, Tiejiong Cao, Meng Sun, and Xiaobing Wang. Detection of people with camouflage pattern via dense deconvolution network. *IEEE Signal Processing Letters*, 26(1):29–33, 2018.
- [8] Zheng Fang, Xiongwei Zhang, Xiaotong Deng, Tiejiong Cao, and Changyan Zheng. Camouflage people detection via strong semantic dilation network. In *Proceedings of the ACM Turing Celebration Conference-China*, pages 1–7, 2019.
- [9] Hung-Kuo Chu, Wei-Hsin Hsu, Niloy J Mitra, Daniel Cohen-Or, Tien-Tsin Wong, and Tong-Yee Lee. Camouflage images. *ACM Trans. Graph.*, 29(4):51–1, 2010.
- [10] Enze Xie, Wenjia Wang, Wenhai Wang, Mingyu Ding, Chunhua Shen, and Ping Luo. Segmenting transparent objects in the wild. In *Computer Vision—ECCV 2020: 16th European Conference, Glasgow, UK, August 23–28, 2020, Proceedings, Part XIII 16*, pages 696–711. Springer, 2020.
- [11] Deng-Ping Fan, Ge-Peng Ji, Tao Zhou, Geng Chen, Huazhu Fu, Jianbing Shen, and Ling Shao. Prant: Parallel reverse attention network for polyp segmentation. In *International conference on medical image computing and computer-assisted intervention*, pages 263–273. Springer, 2020.
- [12] Jiawei Liu, Jing Zhang, and Nick Barnes. Modeling aleatoric uncertainty for camouflaged object detection. In *Proceedings of the IEEE/CVF Winter Conference on Applications of Computer Vision*, pages 1445–1454, 2022.
- [13] Ge-Peng Ji, Lei Zhu, Mingchen Zhuge, and Keren Fu. Fast camouflaged object detection via edge-based reversible re-calibration network. *Pattern Recognition*, 123:108414, 2022.
- [14] Yunqiu Lv, Jing Zhang, Yuchao Dai, Aixuan Li, Nick Barnes, and Deng-Ping Fan. Towards deeper understanding of camouflaged object detection. *IEEE Transactions on Circuits and Systems for Video Technology*, 2023.
- [15] Yunqiu Lv, Jing Zhang, Yuchao Dai, Aixuan Li, Bowen Liu, Nick Barnes, and Deng-Ping Fan. Simultaneously localize, segment and rank the camouflaged objects. In *Proceedings of the IEEE/CVF Conference on Computer Vision and Pattern Recognition*, pages 11591–11601, 2021.
- [16] Nobukatsu Kajiuura, Hong Liu, and Shin'ichi Satoh. Improving camouflaged object detection with the uncertainty of pseudo-edge labels. In *ACM Multimedia Asia*, pages 1–7. 2021.
- [17] Qiang Zhai, Xin Li, Fan Yang, Chenglizhao Chen, Hong Cheng, and Deng-Ping Fan. Mutual graph learning for camouflaged object detection. In *Proceedings of the IEEE/CVF Conference on Computer Vision and Pattern Recognition*, pages 12997–13007, 2021.
- [18] Yujia Sun, Shuo Wang, Chenglizhao Chen, and Tian-Zhu Xiang. Boundary-guided camouflaged object detection. *arXiv preprint arXiv:2207.00794*, 2022.
- [19] Chiyuan He, Linfeng Xu, and Zihuan Qiu. Eldnet: Establishment and refinement of edge likelihood distributions for camouflaged object detection. In *2022 IEEE International Conference on Image Processing (ICIP)*, pages 621–625. IEEE, 2022.
- [20] Jinchao Zhu, Xiaoyu Zhang, Shuo Zhang, and Junnan Liu. Inferring camouflaged objects by texture-aware interactive guidance network. In *Proceedings of the AAAI Conference on Artificial Intelligence*, volume 35, pages 3599–3607, 2021.
- [21] John Canny. A computational approach to edge detection. *IEEE Transactions on pattern analysis and machine intelligence*, (6):679–698, 1986.
- [22] Aixuan Li, Jing Zhang, Yunqiu Lv, Bowen Liu, Tong Zhang, and Yuchao Dai. Uncertainty-aware joint salient object and camouflaged object detection. In *Proceedings of the IEEE/CVF Conference on Computer Vision and Pattern Recognition*, pages 10071–10081, 2021.
- [23] Mengyang Feng, Huchuan Lu, and Errui Ding. Attentive feedback network for boundary-aware salient object detection. In *Proceedings of the IEEE/CVF conference on computer vision and pattern recognition*, pages 1623–1632, 2019.
- [24] Federico Perazzi, Philipp Krähenbühl, Yael Pritch, and Alexander Hornung. Saliency filters: Contrast based filtering for salient region detection. In *2012 IEEE conference on computer vision and pattern recognition*, pages 733–740. IEEE, 2012.
- [25] Kai Han, An Xiao, Enhua Wu, Jianyuan Guo, Chunjing Xu, and Yunhe Wang. Transformer in transformer. *Advances in Neural Information Processing Systems*, 34:15908–15919, 2021.
- [26] Kai Han, Yunhe Wang, Hanting Chen, Xinghao Chen, Jianyuan Guo, Zhenhua Liu, Yehui Tang, An Xiao, Chunjing Xu, Yixing Xu, et al. A survey on vision transformer. *IEEE transactions on pattern analysis and machine intelligence*, 45(1):87–110, 2022.
- [27] Haiyang Mei, Ge-Peng Ji, Ziqi Wei, Xin Yang, Xiaopeng Wei, and Deng-Ping Fan. Camouflaged object segmentation with distraction mining. In *Proceedings of the IEEE/CVF Conference on Computer Vision and Pattern Recognition*, pages 8772–8781, 2021.

- [28] Deng-Ping Fan, Ge-Peng Ji, Guolei Sun, Ming-Ming Cheng, Jianbing Shen, and Ling Shao. Camouflaged object detection. In *Proceedings of the IEEE/CVF conference on computer vision and pattern recognition*, pages 2777–2787, 2020.
- [29] Yujia Sun, Geng Chen, Tao Zhou, Yi Zhang, and Nian Liu. Context-aware cross-level fusion network for camouflaged object detection. *arXiv preprint arXiv:2105.12555*, 2021.
- [30] Qi Jia, Shuilian Yao, Yu Liu, Xin Fan, Risheng Liu, and Zhongxuan Luo. Segment, magnify and reiterate: Detecting camouflaged objects the hard way. In *Proceedings of the IEEE/CVF Conference on Computer Vision and Pattern Recognition*, pages 4713–4722, 2022.
- [31] Shang-Hua Gao, Ming-Ming Cheng, Kai Zhao, Xin-Yu Zhang, Ming-Hsuan Yang, and Philip Torr. Res2net: A new multi-scale backbone architecture. *IEEE transactions on pattern analysis and machine intelligence*, 43(2):652–662, 2019.
- [32] Jia-Xing Zhao, Jiang-Jiang Liu, Deng-Ping Fan, Yang Cao, Jufeng Yang, and Ming-Ming Cheng. Egnnet: Edge guidance network for salient object detection. In *Proceedings of the IEEE/CVF international conference on computer vision*, pages 8779–8788, 2019.
- [33] Ben Niu, Weilei Wen, Wenqi Ren, Xiangde Zhang, Lianping Yang, Shuzhen Wang, Kaihao Zhang, Xiaochun Cao, and Haifeng Shen. Single image super-resolution via a holistic attention network. In *Computer Vision—ECCV 2020: 16th European Conference, Glasgow, UK, August 23–28, 2020, Proceedings, Part XII 16*, pages 191–207. Springer, 2020.
- [34] Sanghyun Woo, Jongchan Park, Joon-Young Lee, and In So Kweon. Cbam: Convolutional block attention module. In *Proceedings of the European conference on computer vision (ECCV)*, pages 3–19, 2018.
- [35] Qilong Wang, Banggu Wu, Pengfei Zhu, Peihua Li, Wangmeng Zuo, and Qinghua Hu. Eca-net: Efficient channel attention for deep convolutional neural networks. In *Proceedings of the IEEE/CVF conference on computer vision and pattern recognition*, pages 11534–11542, 2020.
- [36] Zaiwang Gu, Jun Cheng, Huazhu Fu, Kang Zhou, Huaying Hao, Yitian Zhao, Tianyang Zhang, Shenghua Gao, and Jiang Liu. Ce-net: Context encoder network for 2d medical image segmentation. *IEEE transactions on medical imaging*, 38(10):2281–2292, 2019.
- [37] Zhe Wu, Li Su, and Qingming Huang. Stacked cross refinement network for edge-aware salient object detection. In *Proceedings of the IEEE/CVF international conference on computer vision*, pages 7264–7273, 2019.
- [38] Jun Wei, Shuhui Wang, and Qingming Huang. F³net: fusion, feedback and focus for salient object detection. In *Proceedings of the AAAI conference on artificial intelligence*, volume 34, pages 12321–12328, 2020.
- [39] Shang-Hua Gao, Yong-Qiang Tan, Ming-Ming Cheng, Chengze Lu, Yunpeng Chen, and Shuicheng Yan. Highly efficient salient object detection with 100k parameters. In *Computer Vision—ECCV 2020: 16th European Conference, Glasgow, UK, August 23–28, 2020, Proceedings, Part VI*, pages 702–721. Springer, 2020.
- [40] Xuebin Qin, Deng-Ping Fan, Chenyang Huang, Cyril Diagne, Zichen Zhang, Adrià Cabeza Sant’Anna, Albert Suarez, Martin Jagersand, and Ling Shao. Boundary-aware segmentation network for mobile and web applications. *arXiv preprint arXiv:2101.04704*, 2021.
- [41] Diederik P Kingma and Jimmy Ba. Adam: A method for stochastic optimization. *arXiv preprint arXiv:1412.6980*, 2014.
- [42] Trung-Nghia Le, Tam V Nguyen, Zhongliang Nie, Minh-Triet Tran, and Akihiro Sugimoto. Anabranh network for camouflaged object segmentation. *Computer vision and image understanding*, 184:45–56, 2019.
- [43] Ran Margolin, Lihi Zelnik-Manor, and Ayellet Tal. How to evaluate foreground maps? In *Proceedings of the IEEE conference on computer vision and pattern recognition*, pages 248–255, 2014.
- [44] Deng-Ping Fan, Cheng Gong, Yang Cao, Bo Ren, Ming-Ming Cheng, and Ali Borji. Enhanced-alignment measure for binary foreground map evaluation. *arXiv preprint arXiv:1805.10421*, 2018.
- [45] Deng-Ping Fan, Ming-Ming Cheng, Yun Liu, Tao Li, and Ali Borji. Structure-measure: A new way to evaluate foreground maps. In *Proceedings of the IEEE international conference on computer vision*, pages 4548–4557, 2017.

Received 20 February 2007; revised 12 March 2009; accepted 5 June 2009